Magnetic imaging of a supercooling glass transition in a weakly disordered ferromagnet

WEIDA WU[1,2], CASEY ISRAEL[1], NAMJUNG HUR[2]*, SOONYONG PARK[2], SANG-WOOK CHEONG[2] AND ALEX DE LOZANNE[1]†

[1]Department of Physics, University of Texas, Austin, Texas 78712, USA
[2]Department of Physics and Astronomy and Rutgers Center for Emergent Materials, Rutgers University, Piscataway, New Jersey 08854, USA
*Present address: Department of Physics, Inha University, Incheon 402751, South Korea
†e-mail: delozanne@physics.utexas.edu

Published online: 8 October 2006; doi:10.1038/nmat1743

Spin glasses are founded in the frustration and randomness of microscopic magnetic interactions. They are non-ergodic systems where replica symmetry is broken. Although magnetic glassy behaviour has been observed in many colossal magnetoresistive manganites, there is no consensus that they are spin glasses. Here, an intriguing glass transition in (La,Pr,Ca)MnO_3 is imaged using a variable-temperature magnetic force microscope. In contrast to the speculated spin-glass picture, our results show that the observed static magnetic configuration seen below the glass-transition temperature arises from the cooperative freezing of the first-order antiferromagnetic (charge ordered) to ferromagnetic transition. Our data also suggest that accommodation strain is important in the kinetics of the phase transition. This cooperative freezing idea has been applied to structural glasses including window glasses and supercooled liquids, and may be applicable across many systems to any first-order phase transition occurring on a complex free-energy landscape.

Structural glasses are usually formed by cooling a viscous liquid fast enough to avoid crystallization at the liquid–solid phase transition[1]. Although this phenomenon has been used for many centuries, a quantitative understanding of the glass transition is still a major scientific challenge[2]. Recently, an analogy has been established between the dynamics of structural glasses and that of discontinuous spin glasses[3]. However, it is still an open question whether structural glasses and spin glasses belong in the same family[3]. Spin glasses are disordered systems with frustrated magnetic interactions that result in the absence of conventional long-range order[4,5]. The spin-glass transition is one of the most intriguing problems in condensed-matter physics, where a new type of 'order' arises from breaking an unusual symmetry: the replica symmetry. The spin-glass transition is signified by the deviation of the zero-field-cooled (ZFC) susceptibility $\chi(T)$ from the field-cooled (FC) $\chi(T)$ at the glass-transition temperature, T_G (refs 4,5). Historically, a wider class of heavily doped ferromagnets, for example, transition-metal alloys (CuMn, AuFe, FeAl and so on) have been termed 'cluster glasses' or 'reentrant spin glasses' because they show similar behaviour in $\chi(T)$ below the ferromagnetic (FM) transition[4–7]. It is believed that the magnetization of FM clusters freeze in a random fashion below the glass transition and that the magnetization of each cluster acts like an individual spin in a spin glass, that is, the magnetization of each cluster is free to rotate above the glass temperature. Fundamentally, a cluster glass is a type of spin glass[4]. The most intriguing aspect of these systems is the fact that the FM state appears at a higher temperature than the glass state, indicating that the FM state has larger entropy than the glass state.

Many colossal magnetoresistive (CMR) manganites, especially those exhibiting phase separation, are considered to be disordered ferromagnets. In fact, spin-glass-like behaviour has been found in many CMR manganites[8–13]. It has often been assumed that the isolated FM regions in phase-separated manganites behave like the magnetic clusters in cluster glasses, leading to both CMR effects and glassy behaviour[14,15]. For example, recent experiments

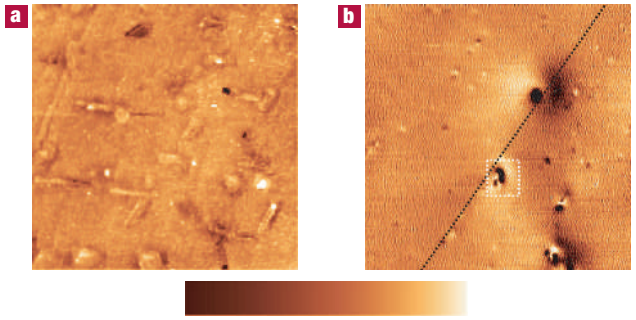

Figure 1 Zero-field images of the same area of the sample ($8 \times 8\ \mu m^2$) taken at 6 K. a, Topography. **b**, MFM. The colour scale is 30 nm for **a** and 150 mHz for **b**. Several small FM droplets can be seen embedded in the non-magnetic CO background. The FM droplets range in size from roughly 100 nm to 1 μm. Although the majority of the smaller FM droplets are single domain, some of the larger FM droplets break up into multi-domain states (one is highlighted by the white dotted box). The magnetization of each FM droplet is oriented randomly. The FM droplets are randomly distributed on the surface, although some of them seem to correlate with twin boundaries (one is marked by the black dotted line) identified by polarized optical microscopy.

show that $La_{5/8-y}Pr_yCa_{3/8}MnO_3$ (LPCMO) ($y \sim 0.4$) has cluster-glass-like behaviour at low temperature[10,11]. However, a real-space microscopic investigation of the glass state has not been carried out to confirm the cluster-glass picture. Here, we carry out variable-temperature magnetic force microscope (VT-MFM) studies on single-crystal LPCMO ($y = 3/8$), a composition in which micrometre-scale phase separation has been observed[16]. The glassy behaviours of our sample have been confirmed by transport and magnetization measurements (see Supplementary Information, Figs S1 and S2). In contrast to the speculated cluster-glass picture, where randomly distributed FM clusters are expected to be seen, we found that the sample has a very small FM volume fraction after ZFC from room temperature to below the glass-transition temperature, T_G (Fig. 1b). The MFM images also show that the FM volume fraction does not change much even with the application of a 1 T field (Fig. 2a). As the temperature approaches T_G during 1 T field-warming (FW), more and more non-magnetic regions are converted to FM domains mostly along orthorhombic twin boundaries (Fig. 3a–e). Near and just above T_G, the FM regions grow into an extensive stripe-like pattern, correlating with the sharp rise in bulk magnetization and the sharp decrease of resistivity. As the temperature is increased further, the phase distribution pattern remains relatively constant with some fraction of the sample remaining non-magnetic (presumably the charge-ordered (CO) phase, which is antiferromagnetic (AFM) below 180 K (ref. 11)) over a wide range of temperature, agreeing with magnetization and resistivity data. In contrast, during the FC–FW process the local phase configuration and therefore magnetization and resistivity are relatively static below the FM transition (Fig. 3g,h). These MFM results and the magnetization data (Fig. 4c) suggest that the low-temperature ($T < T_G$) phase-separated states prepared by different thermodynamic paths arise from the cooperative, dynamic freezing of the first-order AFM(CO) → FM transition (Fig. 4).

Figure 1 shows a typical topographic image and the corresponding MFM image at 6 K after ZFC. The *in situ* resistance is too large to measure at 6 K. The magnetic interaction between the MFM tip and the sample causes a shift of the resonant frequency of the MFM cantilever. The variation of the frequency shift as the tip is scanned across the sample forms the MFM image, as described in the Methods section. Features in the MFM images come from the non-uniform field distribution above the sample surface generated by FM domains. There are several small FM droplets ranging in size from about 100 nm to 1 μm scattered in a non-magnetic matrix, presumably the CO phase. Most of the FM droplets have no correlation with surface defects and orthorhombic twin boundaries (identified by polarized optical microscopy). On the other hand, the twin boundaries act as clear nucleation sites for the AFM(CO) → FM phase change, as shown below. The magnetization of the FM droplets is oriented randomly. Some big droplets have a multi-domain structure to lower their magnetostatic energy. The small fraction of the FM phase agrees well with the *in situ* resistance measurement and *ex situ* both superconducting quantum interference device (SQUID) and resistivity measurements.

At low temperature after ZFC, the CO phase persists unless a field larger than the CO melting field is applied[17]. In Fig. 2, we show a series of MFM images taken during an isothermal magnetic field sweep at 6.8 K after ZFC. During the initial upsweep of the field, no significant increase of the FM fraction is seen below the CO melting field $\mu_0 H_m \approx 2$ T. For fields above 0.5 T, the magnetization of all the FM droplets is aligned with the external field, an observation in agreement with the low magnetic anisotropy and coercive field of three-dimensional manganites[18]. As a moderate field is also enough to align the MFM-tip moment with the external field (as described in the Methods section), the dark colour (negative resonant-frequency shift) in the MFM images corresponds to an attractive interaction between the FM regions and the MFM tip. At $\mu_0 H_m$, the FM regions grow into stripe-like structures aligned parallel to the twin boundaries as the magnetization jumps up (Fig. 2c) and the sample resistance drops to a measurable value (see Supplementary Information, movie S1). The CO phase recedes in a stripe-like fashion at fields up to 2.5 T (see Supplementary Information, movie S1), then disappears after a field increase to 3 T (Fig. 2e). The fact that the bright colour is swept out of the MFM images around $\mu_0 H_m$ gives further credence to our identification of the bright colour as the CO phase. At 3 T the sample is fully FM, with the exception of a few small CO regions probably pinned by defects. The sample then behaves like a conventional isotropic FM with a saturation field of roughly 0.5 T; a subsequent MFM image taken at 1 T (see Supplementary Information, movie S1) shows no changes in the FM state of the sample.

Figure 3 shows two sets of MFM images taken at two locations on the sample during a 1 T FW after ZFC and a 1 T FC. For the ZFC–FW process, images taken from 5 to 16 K show no significant changes and are omitted. Figure 3f shows the temperature dependences of the magnetization of the sample in a 1 T field during FW after ZFC and FC. Comparing MFM images (see Fig. 3a–e and 3g,h, and Supplementary Information, movies S2 and S3, respectively) with magnetization data (Fig. 3f), we conclude that the bulk magnetization is a good measure of the volume fraction of the FM phase at 1 T. The ZFC data in Fig. 3f show a sharp rise in magnetization from 15 to 25 K as MFM images confirm a significant increase in the FM fraction and the *in situ* resistance drops to a finite value. The FM regions tend to grow into stripe-like structures during the transition. For this choice of field (1 T), some CO regions persist above T_G (bright colour at the top centre of the frame in Fig. 3d and e). In contrast to the MFM images taken during ZFC–FW, the FC-FW images (Fig. 3g,h) spanning the same temperature range show that the local phase configuration is relatively static, agreeing with the magnetization data in Fig. 3f.

One common feature in both the melting transition (Fig. 2) and the glass transition (Fig. 3) is that the FM domains form stripe-like features along orthorhombic twin boundaries where a large strain variation is expected. It has been suggested that the micrometre-scale phase separation is caused by the

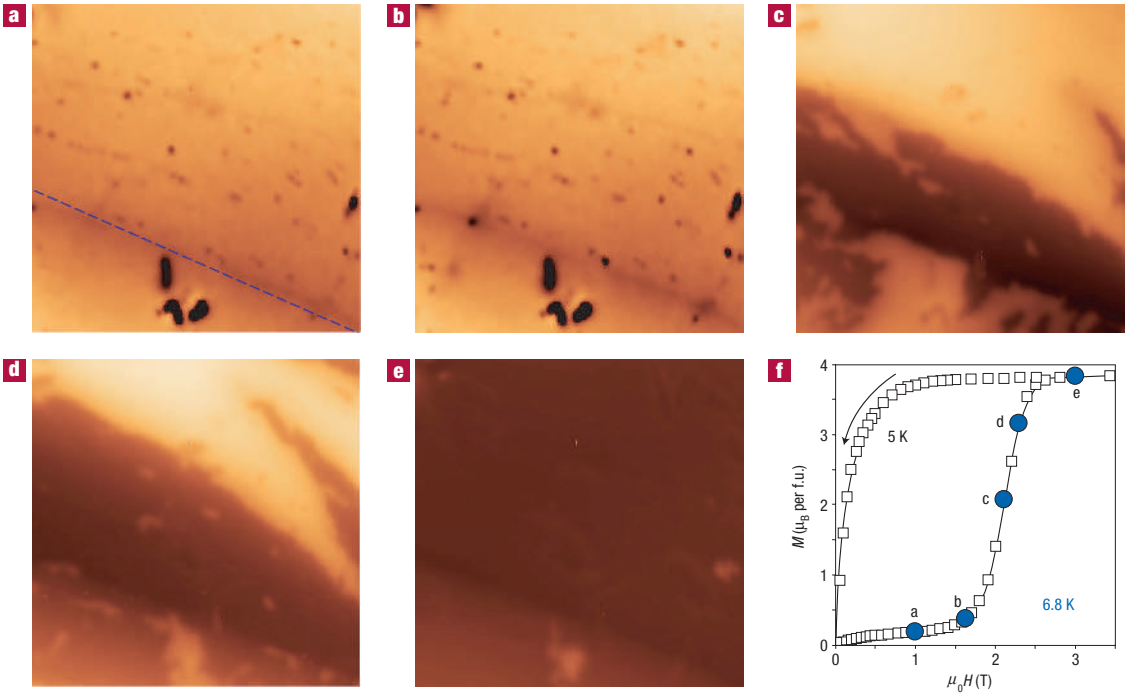

Figure 2 Isothermal magnetic field dependence of MFM images and SQUID magnetization. a–e, MFM images of one area of the sample ($7 \times 7\,\mu m^2$) at various magnetic fields (out-of-plane) at 6.8 K after ZFC. The dashed line in **a** marks the orthorhombic twin boundary seen in polarized optical images (see Supplementary Information, movie S1). The field values (colour scales) of the images are: **a**, 1.0 T (8 Hz); **b**, 1.6 T (8 Hz); **c**, 2.1 T (150 Hz); **d**, 2.3 T (150 Hz); **e**, 3.0 T (150 Hz). **f**, Field dependence of the magnetization (M versus $\mu_0 H$) at 5 K. The filled circles are placed at the field values where the MFM images were taken. The CO melting field is around 2 T. As the melting field is approached and passed, the MFM images show FM regions (dark) appearing and growing at the expense of the CO phase (bright). FM regions form stripe-like structures parallel to twin boundaries. With the application of a 3 T field (**e**), all of the CO phase in the MFM image frame is converted to the FM phase, with the exception of a few small CO regions probably pinned by surface defects. As the field is further lowered to 1 T (see Supplementary Information, movie S1), the sample stays magnetically saturated and (almost) fully FM. This agrees with the magnetization data in **f**.

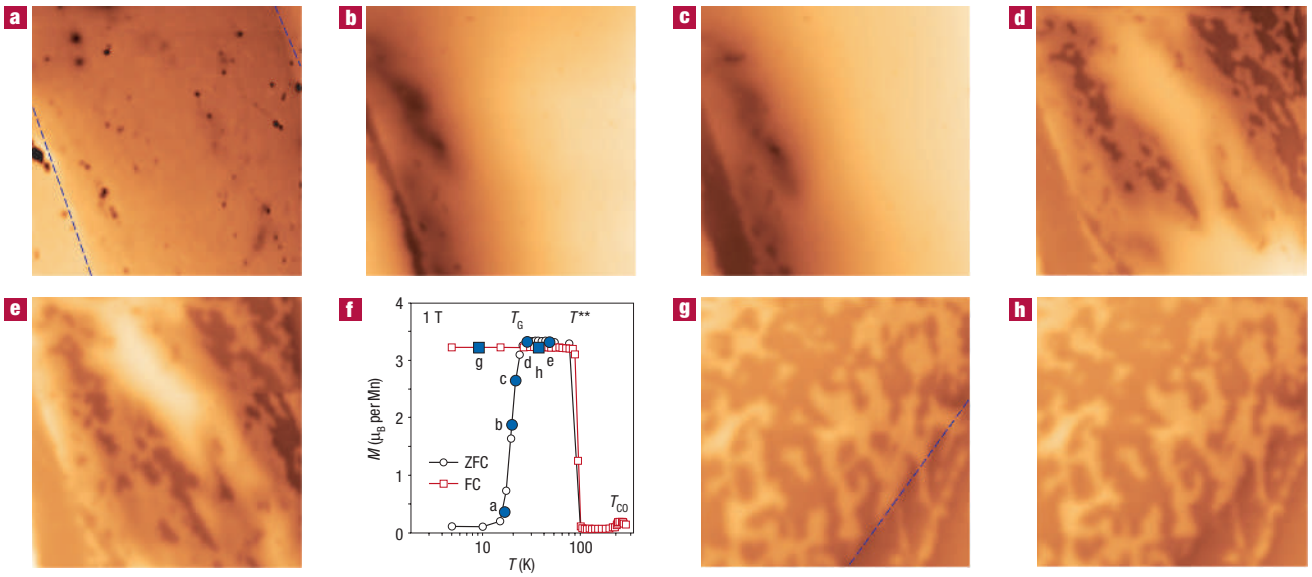

Figure 3 MFM images and magnetization. a–e,g,h, MFM images taken at two locations during FW (1 T) around T_G after ZFC (**a–e**, $6 \times 6\,\mu m^2$) and FC (**g,h**, $7 \times 7\,\mu m^2$), respectively. The dashed lines in **a** and **g** mark the orthorhombic twin boundaries seen in polarized optical images (see Supplementary Information, movies S2 and S3). The magnetic field is out-of-plane. The temperatures (colour scales) of the images are: **a**, 16 K (12 Hz), **b**, 19.4 K (172 Hz), **c**, 21 K (217 Hz), **d**, 25.5 K (172 Hz), **e**, 38 K (141 Hz), **g**, 9 K (100 Hz), and **h**, 35 K (100 Hz). **f**, Temperature dependence of the magnetization (M versus T) during FW after ZFC (open circles) and FC (open squares). The filled symbols mark the temperature of the corresponding MFM images. The glass transition occurs around $T_G \approx 25$ K where the ZFC-FW curve rises sharply to approach the FC-FW curve. The MFM images taken across the glass transition during FC-FW show a relatively static phase pattern with a large FM volume fraction (which develops during FC). Some CO domains (bright contrast) on the sample surface are visible in these images, indicating an incomplete transformation to the FM state.

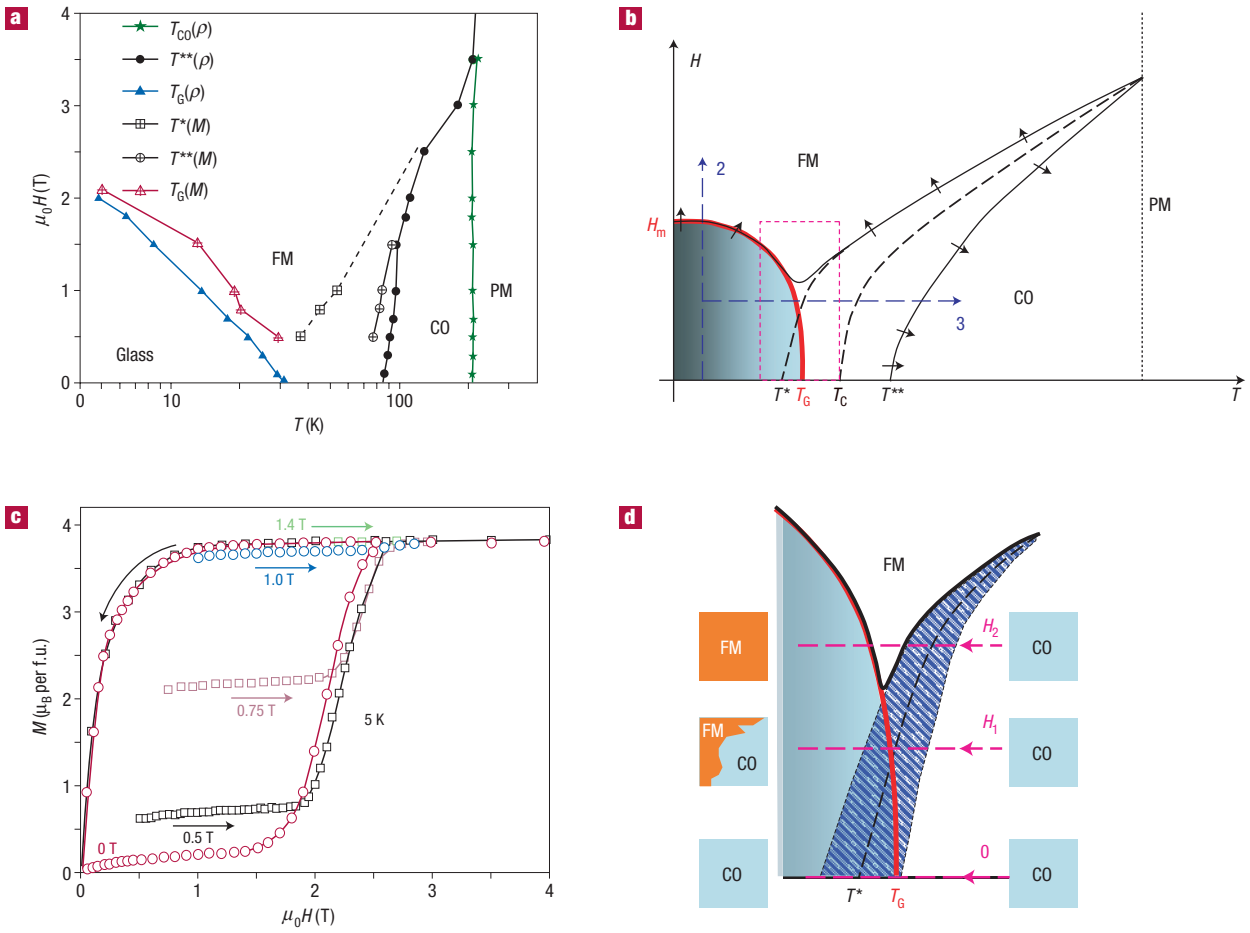

Figure 4 ***H–T* phase diagrams and *M*(*H*) curves after FC. a**, Semi-logarithmic plot of *H–T* phase diagram. See text for definitions of T_C, T^*, T^{**}, T_G and H_m. This phase diagram is constructed with the transport $\rho(T)$ and SQUID magnetization $M(T)$ data in Supplementary Information, Figs S1 and S2. Here the filled symbols are phase boundaries defined by the maximum $d\rho/dT$. The crossed open symbols are boundaries defined by the maximum dM/dT (the 5 K point is taken from the maximum of dM/dH of $M(H)$ in Fig. 2f). The dashed line is a guide for the eye to extrapolate the supercooling line $T^*(H)$ to higher temperature. **b**, A schematic *H–T* phase diagram of LPCMO. The smooth red line from H_m to T_G bounds the 'frozen' state. The combination of $T_G(H)$ and $T^*(H)$ gives rise to a non-monotonic hysteretic boundary. This boundary and T^{**} define the hysteretic phase space as mapped by isothermal field sweeps[11]. The small arrows crossing the hysteretic phase boundaries indicate the direction of the variation of T or H needed for observing the corresponding phase boundary. The blue dashed line labelled 2 (3) represents the thermal paths of the isothermal field sweep (ZFC–FW temperature sweep) shown in Fig. 2 (Fig. 3). **c**, $M(H)$ hysteresis after cooling with various field values: 0, 0.5, 0.75, 1.0 and 1.4 T. The starting magnetization values increase systematically with cooling field values. This illustrates that the supercooling transition ($T^*(H)$) is interrupted systematically by the glass transition ($T_G(H)$), as shown in **d**. **d**, Zoom-in of the phase diagram (marked by pink dashed box in **b**) where $T_G(H)$ and $T^*(H)$ intercept. The hatched area around $T^*(H)$ represents the finite transition width of the supercooling transition. The dashed pink lines represent the thermal paths with different cooling fields ($H_2 > H_1 > 0$). The supercooling transitions at different fields are interrupted by $T_G(H)$ systematically so that the system ends up with different FM volume fractions, that is, different magnetization values.

accommodation strain arising from the lattice mismatch between the FM metallic phase (pseudo-cubic) and the CO insulating phase (orthorhombic)[19]. This point of view is supported by both experiments and simulations[11,20,21]. The correlation between the nucleation and growth of FM domains and orthorhombic twin boundaries suggests that the accommodation strain is important in the kinetics of the phase transition. The anisotropic pattern of the formation of the FM phase can also be understood by the anisotropic nature of the strain interaction. It has been shown that the long-range and anisotropic nature of the strain interaction could generate a complex lattice distortion texture spontaneously, leading to a complex free-energy landscape[21]. It is likely that the cooperative strain interactions frustrate the first-order phase transition in LPCMO.

Figure 4a shows an *H–T* phase diagram for LPCMO constructed from the transport and magnetization data (see Supplementary Information, Figs S1 and S2). Figure 4b is a proposed schematic phase diagram based on MFM studies and Fig. 4a. The thermodynamic first-order AFM(CO) to FM phase transition at T_C has a positive slope ($dH/dT > 0$). The supercooling (superheating) transition temperatures are represented by T^* (T^{**}). It is worth noting the hysteretic nature of T^* (T^{**}); its definition/observation is only valid during cooling (warming). Between T^* and T^{**} there is a hysteretic region where two phases can coexist. The assumed glass-transition temperature T_G is slightly above T^* at zero field. Below T_G, the relaxation is significantly slowed down and eventually stopped, (see Supplementary Information, Fig. S3), that is, the phase transition is frozen, creating a non-ergodic low-temperature state. This metastable state collapses with the application of a large enough magnetic field $\mu_0 H_m$. The combination of $T_G(H)$ and $T^*(H)$ produces a non-monotonic boundary of hysteretic phase space.

To illustrate the frozen states, we measured the magnetization $M(H)$ (Fig. 4c) after cooling in various fields to 5 K. The initial magnetization of the sample increases systematically with the cooling field values, indicating an incomplete AFM(CO) to FM transition interrupted by the glass transition as illustrated in Fig. 4d. For each value of the cooling field, the metastable state collapses to the FM phase at the same $\mu_0 H_m$ as indicated by the sharp rise of the magnetization around 2 T (ref. 17). These non-ergodic states in LPCMO are born from the kinetic freezing of the first-order supercooling transition, implying that the glass transition in LPCMO is a supercooling glass transition that is probably similar to that of structural glasses.

Structural glass transitions have been studied in viscous liquids, polymers and colloidal systems[1]. Despite intensive studies, it is not clear whether this glass transition is a true phase transition blurred by dynamical effects[3], or just a dynamic transition[22]. In this work, we show that a kinetically driven glass transition can also exist in the phase-separated manganite LPCMO. An emerging theme in the manganite community is that both competing phases and quenched disorder are needed to generate both the CMR effect[23–25] and magnetic glassy behaviour[15]. Yet it is under debate whether the CMR manganites are spin glasses[14]. Our MFM results show that the glass state in LPCMO is not a spin-glass state. Instead, it is tightly associated with the supercooled state of the first-order AFM(CO) to FM phase transition, where the kinetics of the phase transition is strongly influenced by the accommodation strain. Because the ionic sizes of La^{3+}, Pr^{3+} and Ca^{2+} are very similar, LPCMO is a weakly disordered FM. It is likely that in this weakly disordered system[12] the accommodation strain, instead of quenched disorder, is responsible for the formation of the complex free-energy landscape[21], where an extensive number of metastable states are separated by effectively infinite barriers. This self-generated complex free-energy landscape is one characteristic of structural glasses[3]. Recently, a magnetic glass state has been observed in the doped ferromagnet $CeFe_2$, in which the kinetic arrest of the first-order FM to AFM transition gives rise to a non-ergodic magnetic state[26]. In principle, it is likely that any system with a first-order phase transition occurring on a complex free-energy landscape can be quenched into a non-ergodic, presumably glassy state. Our results suggest that weakly disordered CMR manganites are not conventional spin glasses where quenched disorder is necessary. The dynamics of this type of magnetic glasses may not be fundamentally different from that of structural glasses.

METHODS

Single-crystal samples of LPCMO ($y = 3/8$) were synthesized in an optical floating-zone furnace. One sample was mechanically cut, polished with 0.1 μm paper with water, and annealed in an O_2 atmosphere at 1,000 °C for 10 h. The surface orientation is [110] in orthorhombic notation, or (100) in cubic notation. The original sample was cleaved into two pieces, one for SQUID measurements and one for VT-MFM and transport measurements. All the MFM images were taken in our homemade instrument, which is inserted into a superconducting magnet before scanning[27]. The VT-MFM is interfaced with a Nanoscope IIIa controller from Digital Instruments. MFM images were taken in a frequency-modulated lift mode, in which the topography and MFM scan lines are interleaved. The lift height ranged from 30 to 40 nm. We used the same lift height within each set of MFM images. It varies a little between different data sets. For images at a different temperature, we maintained the same lift height by compensating for the temperature dependence of the piezoelectric coefficients of the scanner tube. The MFM tip is coated with 25 nm $Co_{85}Cr_{15}$, $\mu_0 H_C \approx 0.05$ T. The MFM tip is magnetized so that the tip moment is normal to the cantilever. The magnetic interaction between the MFM tip and the local magnetization of the sample causes a shift of the resonant frequency of the MFM cantilever, which is recorded as the contrast in the MFM images[27]. Gold wires were attached to the sample by silver paint for resistance measurements taken simultaneously with the MFM data.

The MFM contrast mechanism is set forth in refs 28,29. Briefly, an attractive (repulsive) force on the MFM tip that decays with distance from the sample gives rise to a negative (positive) frequency shift. In the ZFC case of Fig. 1, the local moments of each of the FM regions have a relatively random orientation so that there are both attractive (dark) and repulsive (bright) places, depending on the specific magnetization direction in each region. In a moderate magnetic field, for example, 1 T, the magnetization of both the FM regions in the sample and the MFM tip are aligned with the external magnetic field. Therefore, the only force between them is attractive; the darkest places correspond to regions with the highest effective magnetization[30], averaging over a volume beneath the surface. The absolute value of the resonant frequency depends on temperature, so we generally only show the variation of the resonant frequency in the MFM images.

At room temperature, LPCMO possesses an orthorhombic distortion away from cubic symmetry and forms so-called orthorhombic twins. The optical anisotropy of the orthorhombic lattice can be used to identify different twin domains and the twin boundaries. By matching landmarks in optical images and large area (normally $100 \times 100\ \mu m^2$ or larger) topographic scans taken at room temperature, which contain the topographic regions taken simultaneously with the MFM images at low temperature, we are able to align the MFM images with polarized optical images, as shown in the background of the movies in the Supplementary Information. The twin boundaries are marked by the white dashed lines in the polarized optical images.

Received 20 February 2006; accepted 25 August 2006; published 8 October 2006.

References

1. Debenedetti, P. G. & Stillinger, F. H. Supercooled liquids and the glass transition. *Nature* **410,** 259–267 (2001).
2. Anderson, P. W. Through a glass lightly. *Science* **267,** 1615 (1995).
3. Mézard, M. Statistical physics of the glass phase. *Physica A* **306,** 25–38 (2002).
4. Binder, K. & Young, A. P. Spin glasses: Experimental facts, theoretical concepts and open questions. *Rev. Mod. Phys.* **58,** 801–963 (1986).
5. Mydosh, J. A. *Spin Glasses* (Taylor and Francis, London, 1993).
6. Coles, B., Sarkissian, B. V. B. & Taylor, R. H. The role of finite magnetic cluster in Au-Fe alloys near the percolation concentration. *Phil. Mag. B* **37,** 489–498 (1978).
7. Bao, W. *et al.* Unconventional ferromagnetic and spin-glass states of the reentrant spin glass $Fe_{0.7}Al_{0.3}$. *Phys. Rev. Lett.* **82,** 4711 (1999).
8. Levy, P., Parisi, F., Granja, L., Indelicato, E. & Polla, G. Novel dynamical effects and persistent memory in phase separated manganites. *Phys. Rev. Lett.* **89,** 137001 (2002).
9. Bhattacharya, A., Eblen-Zayas, M., Staley, N. E., Kobrinskii, A. L. & Goldman, A. M. Low-temperature glassy response of ultrathin $La_{0.8}Ca_{0.2}MnO_3$ films to electric and magnetic fields. *Phys. Rev. B* **72,** 132406 (2005).
10. Ghivelder, L. & Parisi, F. Dynamic phase separation in $La_{5/8-y}Pr_yCa_{3/8}MnO_3$. *Phys. Rev. B* **71,** 184425 (2005).
11. Sharma, P. A., Kim, S. B., Koo, T. Y., Guha, S. & Cheong, S.-W. Reentrant charge ordering transition in the manganites as experimental evidence for a strain glass. *Phys. Rev. B* **71,** 224416 (2005).
12. Tomioka, Y. & Tokura, Y. Global phase diagram of perovskite manganites in the plane of quenched disorder versus one-electron bandwidth. *Phys. Rev. B* **70,** 014432 (2004).
13. Deac, I., Diaz, S. V., Kim, B. G., Cheong, S.-W. & Schiffer, P. Magnetic relaxation in $La_{0.250}Pr_{0.375}Ca_{0.375}MnO_3$ with varying phase separation. *Phys. Rev. B* **65,** 174426 (2002).
14. Dagotto, E. *Nanoscale Phase Separation and Colossal Magnetoresistance* (Springer, Berlin, 2003).
15. Dagotto, E. Complexity in strongly correlated electronic systems. *Science* **309,** 257–262 (2005).
16. Uehara, M., Mori, S., Chen, C. H. & Cheong, S.-W. Percolative phase separation underlies colossal magnetoresistance in mixed-valent manganites. *Nature* **399,** 560–563 (1999).
17. Ghivelder, L. *et al.* Abrupt field-induced transition triggered by magnetocaloric effect in phase-separated manganites. *Phys. Rev. B* **69,** 214414 (2004).
18. Salamon, M. B. & Jaime, M. The physics of manganites: Structure and transport. *Rev. Mod. Phys.* **73,** 583–628 (2001).
19. Littlewood, P. Phases of resistance. *Nature* **399,** 529–530 (1999).
20. Pozorov, V., Kim, B. G., Kiryukhin, V., Gershenson, M. E. & Cheong, S.-W. Martensitic accommodation strain and the metal-insulator transition in manganites. *Phys. Rev. B* **64,** 140406 (2001).
21. Ahn, K. H., Lookman, T. & Bishop, A. R. Strain-induced metal-insulator phase coexistence in perovskite manganites. *Nature* **428,** 401–404 (2004).
22. Kurchan, J. In and out of equilibrium. *Nature* **433,** 222–225 (2005).
23. Akahoshi, D. *et al.* Random potential effect near the bicritical region in perovskite manganites as revealed by comparison with the ordered perovskite analogs. *Phys. Rev. Lett.* **90,** 177203 (2003).
24. Burgy, J., Moreo, A. & Dagotto, E. Relevance of cooperative lattice effect and stress fields in phase-separation theories for CMR manganites. *Phys. Rev. Lett.* **92,** 097202 (2004).
25. Motome, Y., Furukawa, N. & Nagaosa, N. Competing orders and disorder-induced insulator to metal transition in manganites. *Phys. Rev. Lett.* **91,** 167204 (2003).
26. Chattopadhyay, M. K., Roy, S. B. & Chaddah, P. Kinetic arrest of the first order ferromagnetic-to-antiferromagnetic transition in $Ce(Fe_{0.96}Ru_{0.04})_2$: formation of a magnetic glass. *Phys. Rev. B* **72,** 180401(R) (2005).
27. Israel, C., Hyun, C., de Lozanne, A. L., Phark, S. & Khim, Z. G. Compact variable-temperature magnetic force microscope with optical access and lateral cantilever positioning. *Rev. Sci. Instrum.* **77,** 023704 (2006).
28. Albrecht, T. R., Grütter, P., Horne, D. & Rugar, D. Frequency modulation detection using high-Q cantilevers for enhanced force microscope sensitivity. *J. Appl. Phys.* **69,** 668–673 (1991).
29. Rugar, D. *et al.* Magnetic force microscopy: General principle and application to longitudinal recording media. *J. Appl. Phys.* **68,** 1169–1183 (1990).

30. Israel, C., Wu, W. & de Lozanne, A. High-field magnetic force microscopy as susceptibility imaging. *Appl. Phys. Lett.* **89,** 032502 (2006).

Acknowledgements

We thank J. Markert for the use of his SQUID and commercial SPM. We benefited from discussions with Q. Niu, P. Chaikin, A. MacDonald, P. Chandra and P. Chaddah. This work is supported by NSF DMR-0308575 (A.dL.) and NSF DMR-0405682 (S.W.C.).
Correspondence and requests for materials should be addressed to A.dL.
Supplementary Information accompanies this paper on www.nature.com/naturematerials.

Author contributions

Crystal synthesis and characterization: N.H., S.P. and S.-W.C. VT MFM design and construction: A.dL. and C.I. Experiment design and planning: W.W., S.-W.C, C.I. and A.dL. Data acquisition and analysis: C.I. and W.W.

Competing financial interests

The authors declare that they have no competing financial interests.